Click Here for Full Article

Model simulation of Greenland Sea upper-ocean variability

S. Häkkinen,[1] F. Dupont,[2] M. Karcher,[3,4] F. Kauker,[3,4] D. Worthen,[5] and J. Zhang[6]

[1] Observations indicate that the occurrence of dense upper-ocean water masses coincides with periods of intense deep-water formation in the Greenland Sea. This paper focuses on the upper-ocean hydrography of the area and its simulation in models. We analyze properties that reside below the summer mixed layer at 200 m and carry the winter mixing signal. The analysis employs numerical simulations from four different models, all of which are forced as specified by the Arctic Ocean Model Intercomparison Project (AOMIP). The models exhibit varying degrees of success in simulating upper-ocean properties observed in the Greenland Sea, including very dense, saline water masses in the 1950s, 1960s, and 1970s. Two of the models predict the importance of salinity in determining the maximum density in the upper waters of the central gyre. The circulation pattern of Atlantic Water was captured well by two high-resolution models as measured by temperature-salinity-density relationships. The simulated temporal variability of Atlantic Water properties was less satisfactory, particularly in the case of salinity.

Citation: Häkkinen, S., F. Dupont, M. Karcher, F. Kauker, D. Worthen, and J. Zhang (2007), Model simulation of Greenland Sea upper-ocean variability, *J. Geophys. Res.*, *112*, C06S90, doi:10.1029/2006JC003687.

1. Introduction

[2] Modeling the Nordic Seas, and the Greenland Sea in particular, is a challenging task because the area is characterized by a complex system of exchanges among adjacent oceans and strong topographic influence on ensuing processes. The last 50 years have seen large fluctuations in the stratification structure of the Greenland Sea. Years prior to 1980 were dominated by a weakly stratified, domed structure whose center was filled with newly formed Greenland Sea Deep Water (GSDW). Since 1980, the domed structure has gradually flattened and is associated with warming of GSDW due to lack of deep convection [*Schlosser et al.*, 1991; *Bonisch et al.*, 1997; *Budeus et al.*, 1998; *Osterhus and Gammelsrod*, 1991; *Karstensen et al.*, 2005]. The new approach of using chlorofluoromethanes F11 and F12 to measure ventilation of deep waters showed that the renewal rates had significantly decreased by 1993 and especially from the reference period of 1982–1989 [*Rhein*, 1991, 1996]. As the central gyre has grown fresher and more stratified since the mid 1980s, warming of the core of the incoming Atlantic Water has accelerated [*Blindheim and Osterhus*, 2005, Figure 6]. These trends would require extremely large buoyancy losses in order to return the

Greenland Sea upper (and lower) ocean stratification to the conditions prior to 1980.

[3] The focus of this study is to investigate how well we can simulate upper-ocean conditions of the Greenland Sea because we presume that preconditioning of the upper ocean is important for dense water production. With increasing density in the upper ocean there is a corresponding increase in the likelihood that deep-water formation can occur. Arctic Ocean simulation depends upon adequate simulation of upper-ocean conditions in the Nordic Seas. Exchanges between the North Atlantic and Arctic Oceans are thought to influence Nordic Seas processes as much as local forcing. Modified Atlantic Water continues to the Arctic, where it undergoes further modification before emerging again beneath the surface in the Nordic Seas. Thus, capturing upper-ocean variability in the Greenland Sea in particular is a preamble for successful Arctic Ocean simulation.

[4] Our model simulations incorporate results from models limited to the Arctic and Nordic Seas as well as models with an active connection to the North Atlantic Ocean. In principle, temperature simulation should be successful because the upper-ocean heat content is in equilibrium with the local atmospheric flux on seasonal time scales. A complication is presented by advection of heat from the main North Atlantic Ocean, which provides a major contribution to the heat balance in the Nordic Seas. Advection is even more critical for the salt balance, which, combined with not-so-well determined fluxes of fresh water and runoff, makes successful simulation of salinity difficult. One measure of model success at simulating interaction with the North Atlantic is the timing and amplitude of the Great Salinity Anomaly [*Dickson et al.*, 1988], which started its passage through the Nordic Seas around 1976–1978. It will become apparent that the models discussed are

---

[1]NASA Goddard Space Flight Center, Greenbelt, Maryland, USA.
[2]Quebec-Ocean, Université Laval, Sainte-Foy, Québec, Canada.
[3]O.A.Sys. - Ocean Atmosphere Systems GbR, Hamburg, Germany.
[4]Alfred Wegener Institute for Polar and Marine Research, Bremerhaven, Germany.
[5]Science Systems and Applications Inc., Lanham, Maryland, USA.
[6]Applied Physics Laboratory, University of Washington, Seattle, Washington, USA.

far from perfect, but progress toward higher resolution may eventually improve their simulations.

[5] Sections 2 and 3 of this paper provide general descriptions of models and surface forcing, respectively. Section 4.1 probes mutual relationships between salinity, temperature, and density fluctuations, and section 4.2 discusses time evolution through the center of the Greenland Sea convection area (75°N). Section 4.3 explores whether the simulated upper-ocean density maximum along 75°N is related to salinity, as observations suggest, or to temperature. The simulated Atlantic Water properties are discussed in section 4.4.

2. Models

[6] The models surveyed here are from Alfred Wegener Institute (AWI), Goddard Space Flight Center (GSFC), University of Laval (UL), and University of Washington (UW). The AWI, UL, and UW models are all based on the Modular Ocean Model (MOM). The UW model is a parallel ocean program (POP) based on MOM architecture originally developed at the National Oceanic and Atmospheric Administration's Geophysical Fluid Dynamics Laboratory; it implements z-levels in the vertical and B-grid in the horizontal directions. The GSFC model is based on the Princeton Ocean Model (POM) developed by G.L. Mellor and colleagues [*Blumberg and Mellor*, 1987] and uses terrain-following sigma-coordinates and C-grid in the horizontal. All these ocean models were run coupled to a dynamic-thermodynamic ice model; however, the associated ice model results were not used for this analysis because surface salinity flux constitutes only a small contribution to the local subsurface salt balance when compared to salt advection. Table 1 lists pertinent discretization properties of the models analyzed. Publications relevant to choices of parameters and other information include *Karcher et al.* [2007] for the AWI model; *Häkkinen and Mellor* [1992] and *Häkkinen and Geiger* [2000] for the GSFC model; *Holloway and Sou* [2002] for the UL model (note that the UL model is a domain-extended version—the southern border crosses the North Atlantic from Newfoundland to France of *Holloway and Sou* [2002]); and *Zhang et al.* [2000] and *Zhang and Steele* [2007] for the UW model. There is an extensive summary of model parameters in *Holloway et al.* [2007]. Observations were retrieved from NOAA/NODC (National Ocean Data Center) and International Council for the Exploration of the Sea (ICES) hydrographic data archives. The specific subset of observational data used in this study is discussed by *Häkkinen* [2007].

3. Forcing

[7] All the models use forcing as defined by the Arctic Ocean Model Intercomparison Project (AOMIP) with some exceptions. The forcing is based mostly on the National Centers for Environmental Prediction/National Center for Atmospheric Research (NCEP/NCAR) Reanalysis data. Forcing for most atmospheric quantities has a daily temporal resolution, except in the UL model, which uses monthly data. Detailed specifications of the NCEP-derived forcing are given on the AOMIP Web site: http://fish.cims.nyu.edu/project_aomip/overview.html. For instance, wind stress over the Arctic is computed directly from geostrophic winds, which are derived from sea-level pressures with fixed rotation depending on the wind speed. All models use the heat exchange coefficient of 1.2E-3 for sensible and 1.5e-3 for latent heat, and the formulation for net long-wave radiation by *Rosati and Miyakoda* [1988]. There is some variety in the short-wave radiation and in the albedos for ice, snow, and melting ice and snow [see *Holloway et al.*, 2007, Appendix A].

[8] Precipitation is implemented from the Serreze and Hurst (2000) data set for limited-area models (UW, AWI, UL), but for larger-scale models (GSFC) an option is to use other global products [e.g., *Xie and Arkin*, 1996] or data sets these models have used previously. For instance, the GSFC model uses *Rasmusson and Mo* [1996] P-E fields supplemented with extra water at the Intertropical Convergence Zone to prevent excessive drift of the average salinity in the model. For bathymetry in very high-resolution models, International Bathymetric Chart of the Arctic Ocean data was used together with the Earth Topography Five Minute (ETOPO5) data set for areas outside the Arctic. The coarse-resolution GSFC model used TerrainBase Digital Terrain Model with heavy smoothing. River runoff data is drawn from the hydrographic data product for the Arctic region developed at the University of New Hampshire [*Lammers and Shiklomanov*, 2000], except in large-domain models (GSFC), data from the Global Runoff Data Center (Koblenz, Germany) is used (however, the former data set relies on the same Russian, U.S., and Canadian tide gauge data as the latter).

[9] The hydrography needed for ocean-model initialization is acquired from a global merged data product, where various high-quality Arctic Ocean data sets have been blended with the World Ocean Atlas [*Steele et al.*, 2001]. Net transport at open boundaries is such that inflow through the Bering Strait is 0.8 Sv in the GSFC model and 1 Sv in the UL model, with the same amount flowing out through the southern boundary (15°S in GSFC and ~50°N in UL). The Bering Strait is closed in the AWI model. At the southern boundary, near 50°N, where the net flow is zero, the open boundary condition is a constant (in time) barotropic flow taken from a coarse-resolution, larger-scale version of the same AWI model. Boundary T and S for the calculation of baroclinic flows are derived from *Steele et al.* [2001]. The UW model has open boundaries at the

Table 1. Discretization Properties of the Models Analyzed[a]

Model	Type	Vertical Grid	Horizontal Grid	Horizontal Resolution
AWI	MOM	z-level, 33 levels	B grid	0.25 × 0.25 degrees
GSFC	POM	σ-coord. 20 levels	C grid	0.7 × 0.9 degrees
UL	MOM	z-level 29 levels	B-grid	1/2 × 1/2 degrees
UW	MOM/POP	z-level 25 levels	B-grid	0.36 × 0.36 degrees

[a]Model domains: AWI, 50°N to Bering Strait; GSFC, 15°S to Bering Strait; UL, approximately 50°N (Newfoundland to France) to Bering Strait; UW, Nordic Sills to Bering Strait. Temporal coverage of data: AWI, 1948–1999; GSFC, 1948–2001; UL, 1950–1999; UW, 1948–2001. Observations: 1951–2000.
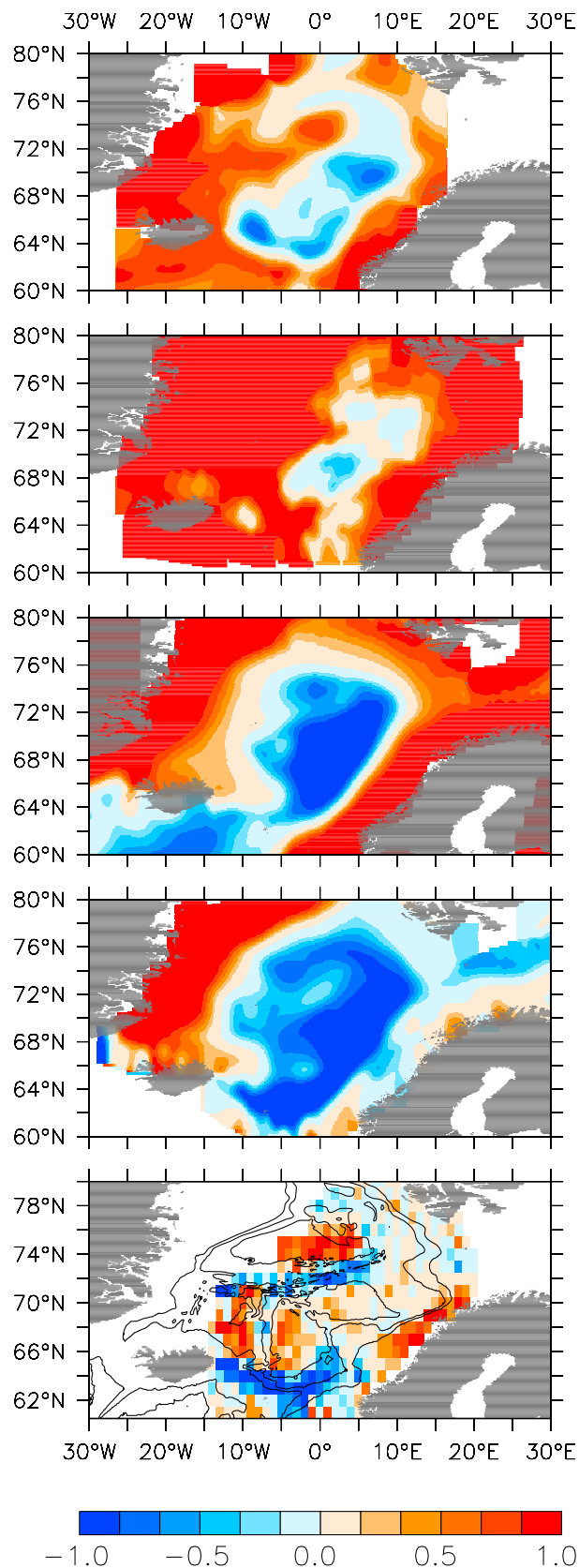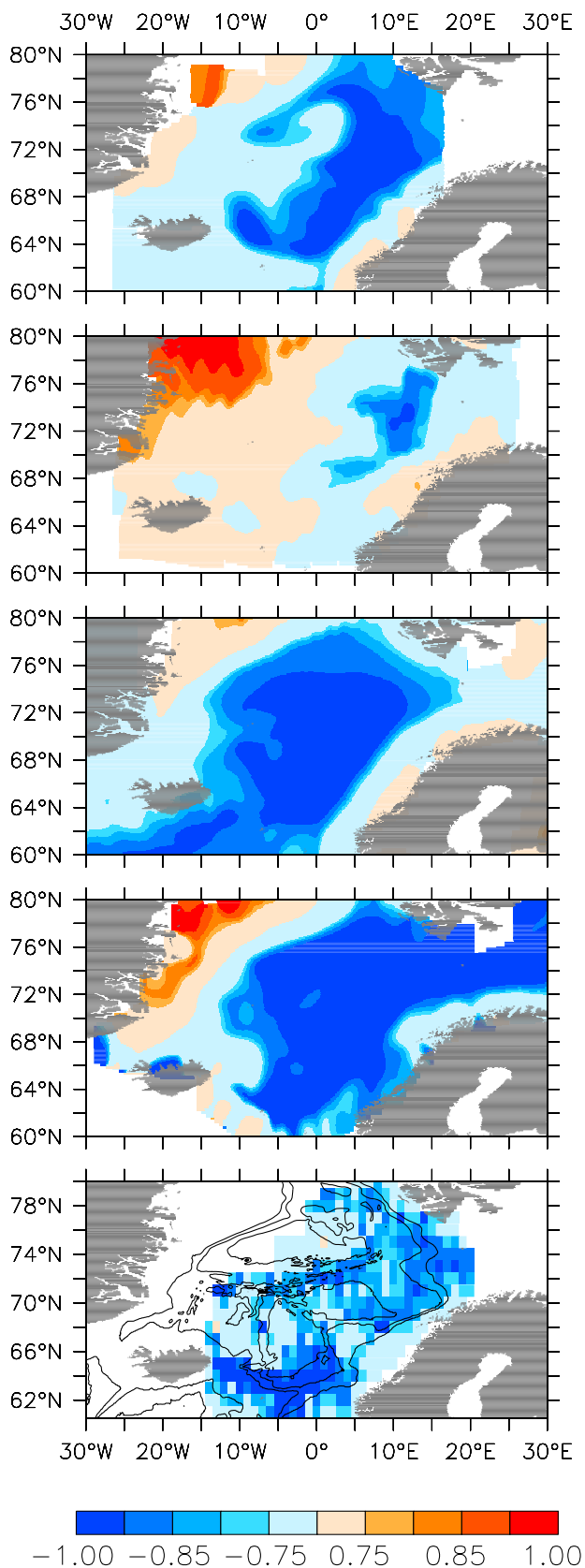
Figure 1. Correlations between salinity and density are shown for 200 m depth from the (a) AWI, (b) GSFC, (c) UL, (d) and UW models, and (e) observations. Isolines in (e) refer to water depth with intervals of 1000 m. Based on record lengths as defined in Table 1.

Bering, Davis, and Denmark Straits and the Iceland-Shetland Pass. Its open boundary conditions for hydrography, velocities, and sea-surface heights were obtained from a global version of the same UW ice-ocean model using NCEP/NCAR Reanalysis forcing fields [*Zhang and Rothrock*, 2003]. Following the protocol for the AOMIP-coordinated experiment, the AWI and UW models use surface salinity restoring for the first 10 years, after which the models evolve freely, while no restoring is used in the GSFC or UL models.

4. Results

4.1. T-S-RHO Relationships

[10] We first investigate the relationships between fluctuations of hydrographic properties to highlight the different water masses and their routes. We use primarily summertime data because hydrographic observations are most abundant during summer. It is assumed that the summertime data retains a memory of the previous winter's effects on hydrography below the shallow summer mixed layer. We use data from 200 m depth, with the exception of 234 m depth for the UW model. This depth level is within the winter mixed layer in most of the Greenland Sea, so hydrographic properties at this depth serve as a proxy for winter conditions in the upper ocean. The model and observed data are binned into summer-month averages (May–September); however, UL model data was available only as an annual average. (Results are not significantly different for annually averaged data, but use of summer data stems, as noted, from availability of observations.) The salinity-density relationship is known to be important at high latitudes, but, in fact, this holds true only in the cold Arctic waters and in a few isolated ice-free areas. Figures 1a–1d show correlations of salinity and density over the 50–54-year data period available as calculated by the different models after removal of the linear trend; Figure 1e shows the observed relationship. Only the AWI and GSFC models show a positive correlation in the central Greenland Sea as expected from observations. Interestingly, the positive correlations observed at the Norwegian Coast (reflecting the fresh Norwegian Coastal Current) are also present in all the models, but the weakest signal is in the UW model. The negative correlations denoting fluctuations of Atlantic origin waters are captured by all the models and are located approximately along the path of the Norwegian Atlantic Current south of 66°N. The UL and UW models carry the negative correlations around the Greenland basin to the central gyre. This means that the simulated Atlantic Water mass in the UL and UW models retains an excess of its original properties (i.e., minimal cooling and freshening). The AWI and UW models, the two with the highest resolution, are the most similar in spatial patterns that exhibit a distinctive spiral path of low/negative correlations belonging to the Atlantic Water. In the GSFC model, the pattern of negative correlations is broad, diffuse, and lacking detail. The observed close connection to the ridges separating the basins is not well defined in any of the models: Compared to the observations, all the models lack the signal of Atlantic Water flow under the Jan Mayen Current along the Mohn Ridge.
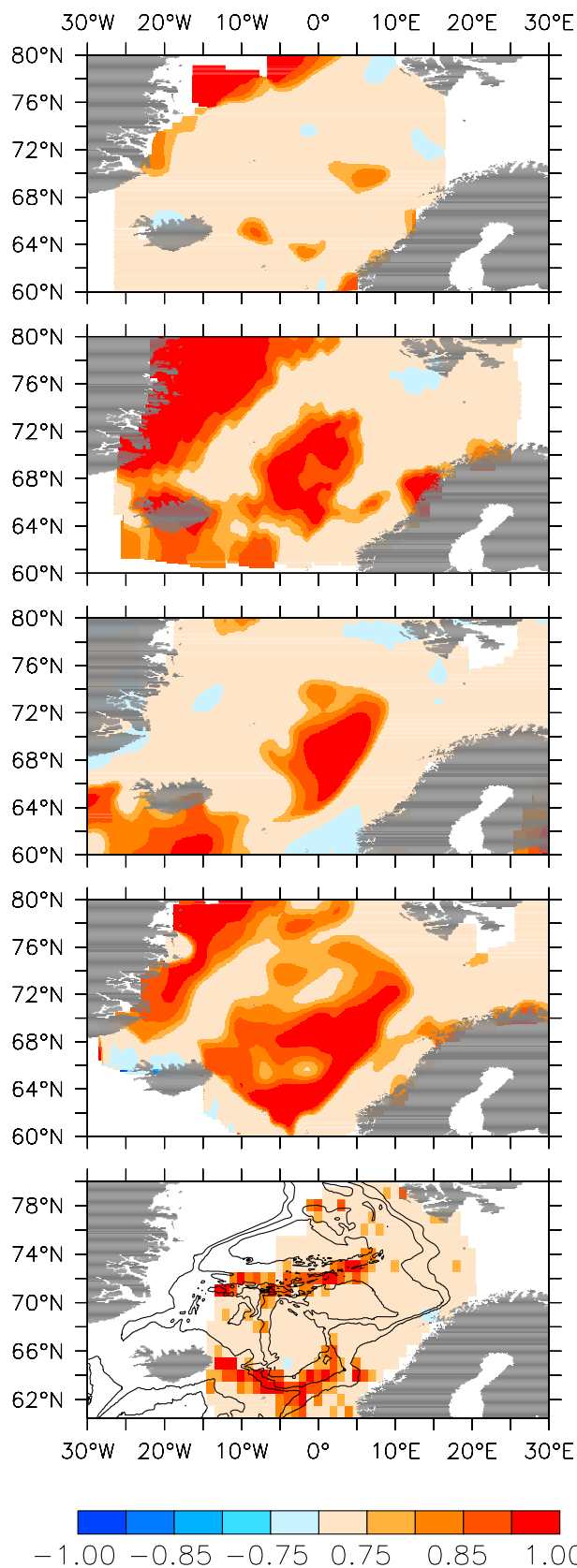
[11] The temperature-density relationship emphasizes the paths of the Atlantic Water and its mixed products. The modeled temperature-density correlations are given in Figures 2a–2d, and the observed ones in Figure 2e. The AWI model appears to be the best at showing the spiraling of Atlantic Water around the periphery of the Greenland Basin. The UL and UW models retain too much Atlantic Water in their central gyres, while GSFC shows too weak a signal for Atlantic Water along the observed path of the Norwegian Atlantic Current. Even though we don't have sufficient observational data on the western side of the Nordic Seas, most of the models seem to indicate a positive correlation in the northwest corner of the region. In this same region, all the models show the salinity-density relation to be tightly coupled; hence a positive correlation with temperature-density changes of the same sign would indicate mixing of cold, fresh waters with warm, saline waters, with the end product being warmer and saltier.

[12] Finally, we present the mutual relationship between salinity and temperature (Figure 3), which describes the conservation of water mass characteristics, e.g., that of Atlantic Water. In the observations (Figure 3e), incoming Atlantic Water rapidly loses its salinity signature because it mixes with freshwater sources from the East Iceland Current, precipitation, sea-ice melt, and runoff [*Blindheim and Osterhus*, 2005, Figure 7]. Remarkably, only the extension of the Norwegian Atlantic Current along Mohn Ridge conserves its properties until it turns northward along the eastern rim of the Greenland Basin. Since mixing with ambient fresh waters and freshwater fluxes defines the T-S correlation, it is not surprising that the model results show rather different-looking patterns from those observed. The topographic control of the flows (whereby the flow tends to follow f/H contours) appear to be inadequately simulated, suggesting that the simulated stratification is too strong, allowing the upper-ocean currents to feel only weakly the potential vorticity gradients imposed by topography.

4.2. T-S-RHO Time Evolution

[13] To follow the time variability of the hydrographic properties, we chose 75°N latitude and a longitude span of 8°W to 15°E, because this section includes the center of the Greenland Sea gyre and the center of convective activity, which is considered to be in the vicinity of 0°E, 75°N [*GSP Group*, 1990]. The observed data were too sparse to create a continuous time series extending farther than 8°W to capture the full extent of the recirculating Atlantic Water, which exhibits the warmest temperatures between 10°W and 12°W at 200 m [*Drange et al.*, 2005, Figure 8]. Starting from the temperature evolution shown in (Figure 4), the simulated water masses across the section in all models are considerably warmer than the observations; the Atlantic Water tends to be at least 1°C warmer than observations. In two models (UW and UL), the warm Atlantic Water dominates the whole central gyre. The GSFC model depicts the closest match with observations for the timing (see also Figure 8a), but not the amplitude of the decadal temperature fluctuations in Atlantic Water.

[14] Comparison of simulated values with observed salinity is less successful than comparison for temperature in all models (Figure 5). Significant salinity drift is apparent in several models which try to adjust to specified surface

Figure 2. Correlations between temperature and density are shown for 200 m depth from the (a) AWI, (b) GSFC, (c) UL, (d) and UW models, and (e) observations. Isolines in (e) refer to water depth with intervals of 1000 m. Based on record lengths as defined in Table 1.

Figure 3. Correlations between temperature and salinity are shown for 200 m depth from the (a) AWI, (b) GSFC, (c) UL, (d) and UW models, and (e) observations. Isolines in (e) refer to water depth with intervals of 1000 m. Based on record lengths as defined in Table 1.
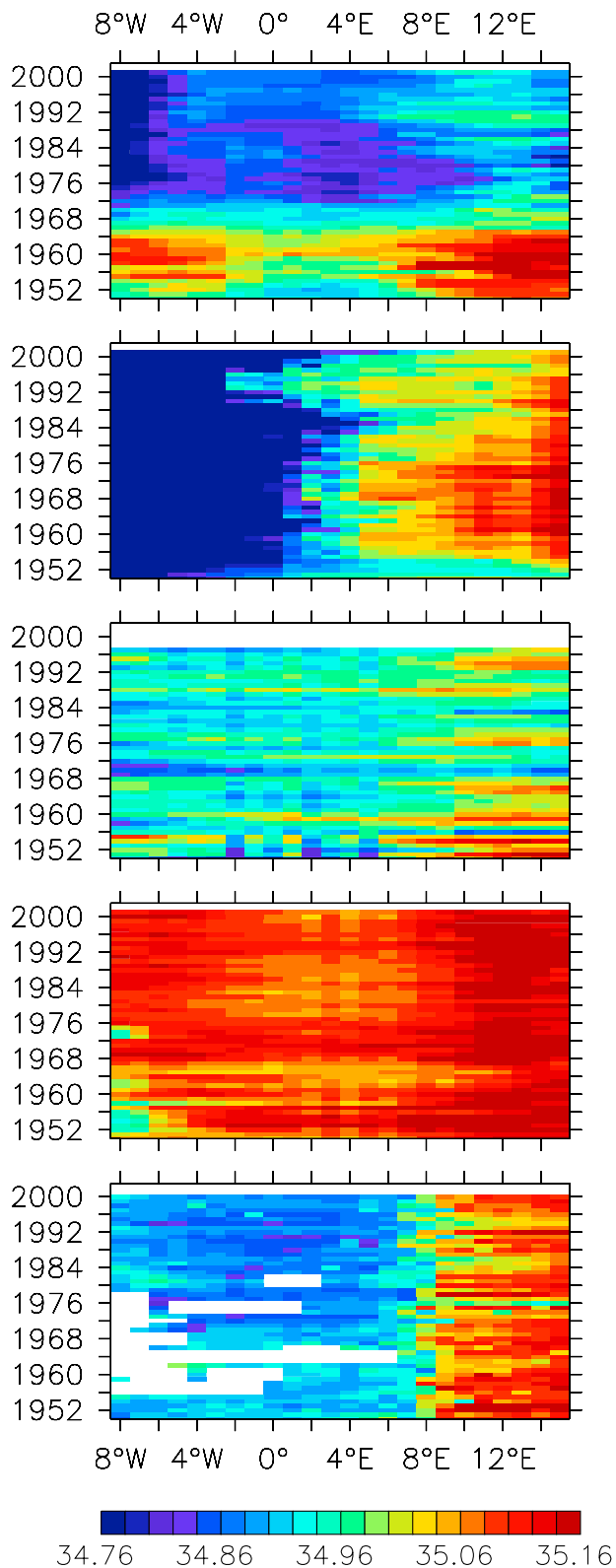
Figure 4. Hovmueller diagrams for temperature along 75°N (all data within ±1.5° [latitudes] 75°N are averaged) for the (a) AWI, (b) GSFC, (c) UL, and (d) UW models, and (e) from observations.
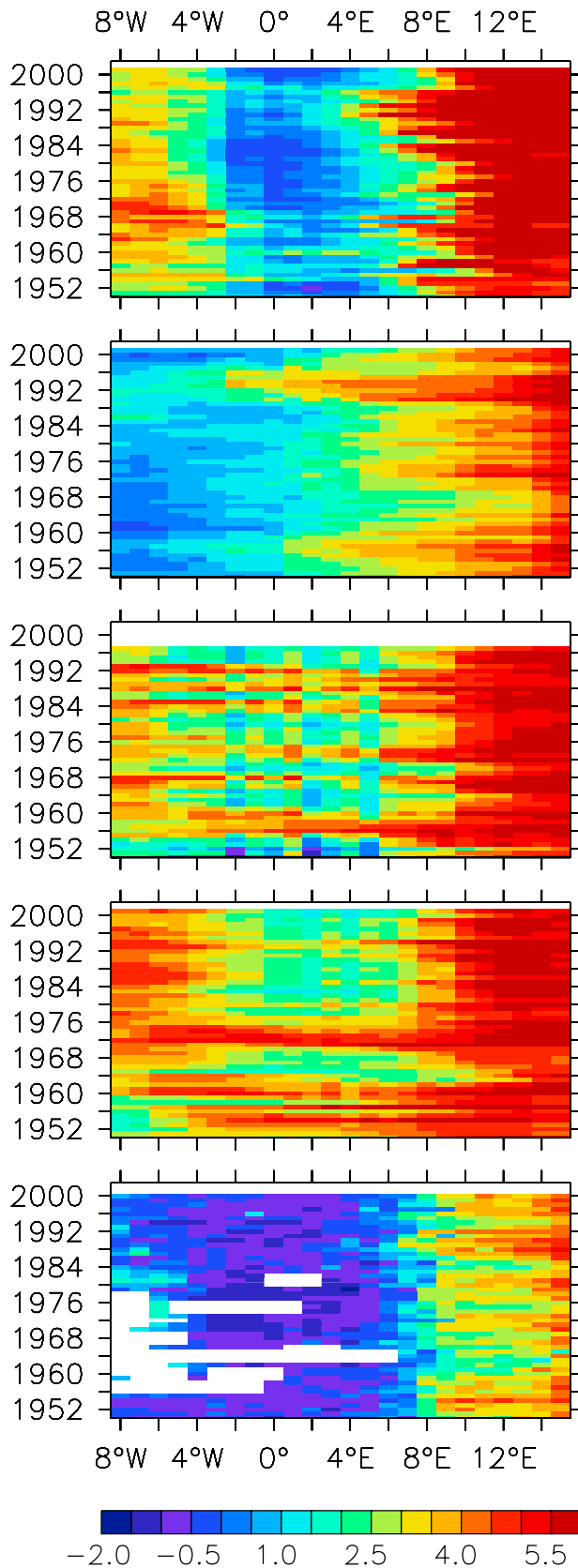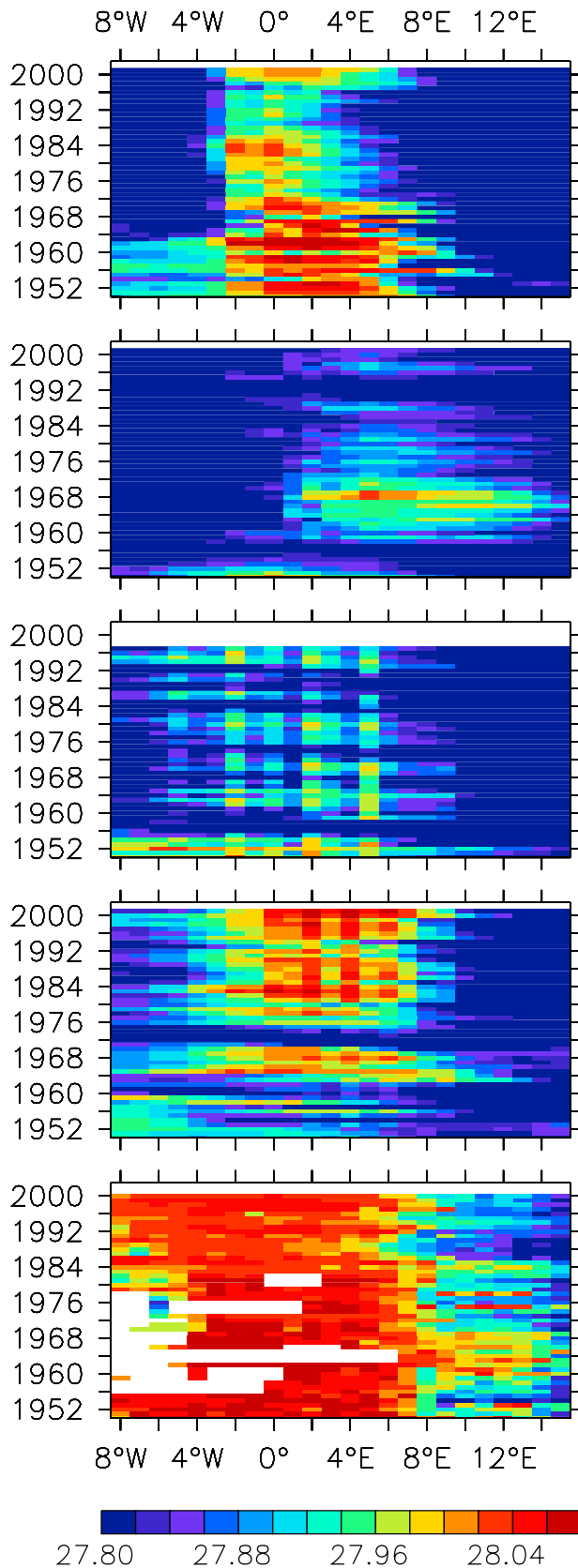
Figure 5. Hovmueller diagrams for salinity along 75°N (all data within ±1.5° [latitudes] of 75°N are averaged) for the (a) AWI, (b) GSFC, (c) UL, (d) and UW models, and (e) observations.

freshwater inputs under restrictive climatological open boundary conditions. Removal of salinity restoring after 10 years can further enhance the drift as in AWI. The overall level of salinities ranges significantly; for example, the UW model is more saline than the observations or any of the other models across the central basin. Atlantic Water in the UL model is much fresher than in the other three models, with a weak east–west contrast; however, this model shows vigorous variability on a decadal scale. The GSFC model is very fresh at the beginning of the simulation, but recovers fully to realistic values of salinity in the Atlantic Water domain, although the domain extends farther west than observed. The GSFC model maintains an intense east–west salinity gradient, which is stronger than in the observations. In the AWI model, there is a transition from saline to fresh conditions in the late 1960s, which can be attributed to a shift in surface salinity forcing from restoring to nonrestoring conditions, and this trend persists for the remainder of the simulation. Without restoring of surface salinity the model is bound to drift on the long-term if there is any misfit between model physics and applied forcing data sets (e.g., net precipitation). Observations show the salinities in the 1960s to be much higher than at any time afterward (Figure 5e and also seen in Figure 7i and Figure 10a); however, the observational trends are much weaker than trends in the GSFC and AWI models. In the GSFC model the Atlantic inflow remains reasonably saline throughout the simulation, though it lacks the strong decadal fluctuations of the observed record.

[15] Density evolution from the models (Figure 6) reveals that despite the deficiencies in T and S evolution, the simulated long-term variability in at least some of the models (AWI, GSFC) shows the same sign of a trend as the observations (Figure 6e): The densest water masses are found in the 1960s and 1970s in the central gyre with a gradual trend towards a lighter upper ocean. Here again the model trends are much stronger than observed. The UL model shows decadal fluctuations in the central gyre that are not present in the observed record. The UW model has a persistent trend toward denser waters at 234 m during the 50-year simulation. None of the models achieves densities as heavy as those found in the observations.

4.3. Salinity- or Temperature-Driven Regime in the Central Gyre?

[16] Another aspect of analyzing the simulated density evolution at 200 m concerns whether the maximum density fluctuations (along 75°N) are determined by changes in temperature or in salinity, and whether this relationship changes with time. We locate the maximum density along 75°N (from data displayed in Figure 6) and the associated T and S. The T-S-RHO relationships for the models and observations are shown in Figure 7. The AWI model, Figure 7a, shows the 200-m density maximum each year (in summer) and the maximum salinity. During the first half of the record until about 1977, the density fluctuations are determined by salinity fluctuations. After about 1977, the maximum density appears to follow temperature fluctuations (Figure 7b). Thus the AWI model shifts its mode of operation in the late 1970s by transitioning its densest upper-ocean waters from a salinity-dominated regime to a temperature-dominated regime. In the GSFC model after

Figure 6. Hovmueller diagrams for density along 75°N (all data within ±1.5° [latitudes] of 75°N are averaged) for the (a) AWI, (b) GSFC, (c) UL, (d) and UW models, and (e) from observations.

the major adjustment at the beginning, i.e., after 1960, the density maximum follows the salinity evolution (Figure 7c), although there are exceptions; the 1991–1992 low-density event was caused by intrusion of very warm temperatures (Figure 7d). The GSFC density maximum/temperature relationship (Figure 7d) shows that the adjustment at the beginning of the simulation was governed by temperature effects. In the UL and UW models the density maximum is determined by temperature effects (Figures 7e–7h), with salinity variations being out-of-phase (high salinity – low density). These model behaviors should be contrasted with observations, in which the density maximum is always determined by salinity, while the temperature effect is not very apparent as shown in Figures 7i and 7j.

[17] The models exhibit some difficulty with capturing the fundamental characteristics of upper-ocean density fluctuations, at least in these hindcasts for the last 50 years. The subtle interaction of salt and heat content, the buoyancy loss, and the influence of advected heat and salt pose a major challenge to the models. Of course, it is possible that these diagnostics of hydrographic relationships may not work for periods longer than 50 years, since we do not have long enough records of observations to determine whether and how often dense water formation may shift from a salinity-dominated regime to a temperature-dominated one.

4.4. Atlantic Water

[18] The salinity of central Greenland Sea waters is extremely important to upper-ocean density fluctuations in the central gyre as seen in Figure 7i. One has to assume that the hydrographic properties of incoming Atlantic Water play a critical role in the water mass modification process. Figures 8a and 8b present a detailed evolution of Atlantic Water temperature as calculated by various models at 200 m depth at 15°E, 75°N. Please note that at 75°N the Atlantic Water has already passed through a large part of the eastern Norwegian Sea after its inflow over the Iceland and Scotland Ridges. The UW and GSFC models fare rather well compared to observations, with correlations of 0.40 and 0.53, respectively (both significant at the 95% level for detrended data), but fluctuation amplitudes are damped. The AWI model develops the largest offset with respect to observational values, and thus it exhibits no significant correlations. However, employing restoring of surface salinity to climatology in the AWI model gives good results for comparison of the model's results and observations in the timing and amplitude of temperatures in the Atlantic Water branches of the Nordic Seas [e.g., *Karcher et al.*, 2003; *Polyakov et al.*, 2005]. One immediate observation is that a large initial adjustment directs the models rapidly away from their initial conditions after the first decade, during which the GSFC, AWI, and UW models all show similarity with the observations. One would have hoped that long-term use of similar surface forcing would at least give similar evolution, but in the incoming Atlantic Water region advection is an important part of the ocean heat balance. In an equilibrium, net heat loss is compensated by oceanic advection of heat in the whole water column in any grid box:

$$\int_{-h}^{0} \left[(uT)_x + (vT)_y \right] dz = -Q / \rho\, C_p$$

where Q is the net annual heat flux, u,v are the velocity components, C_p is the specific heat of water, and h is the water depth. It should be obvious that in areas like the Greenland-Iceland-Norwegian Seas, which are dominated by net heat loss, the long-term heat balance must be achieved by advection of heat. To gauge the amount of advected heat needed beyond the seasonal heat gain to close the annual balance, a ratio of average winter heat loss over average summer heat gain is computed. This ratio highlights the importance of local effects (heat flux) and remote effects (advected heat) in each grid point as shown in Figures 9a–9d, based on 45 years (1955–1999) of model surface fluxes.

As a long-term average, the AWI, UL, and GSFC models are similar in their depiction of higher ratio values along the Atlantic Water path, but details of the magnitude of the ratio and the location of the maximum values are quite different. Ratios in the UW model differ significantly from those in the rest of group for unknown reasons. If the surface heat fluxes were exactly the same in each model, advection would be the only reason for differences. As noted, Atlantic Water temperatures are too warm in all models, which influences surface flux forcing that in turn feeds back to the ocean temperatures. However, the model feedbacks that lead to differences in surface heat fluxes do not negate the
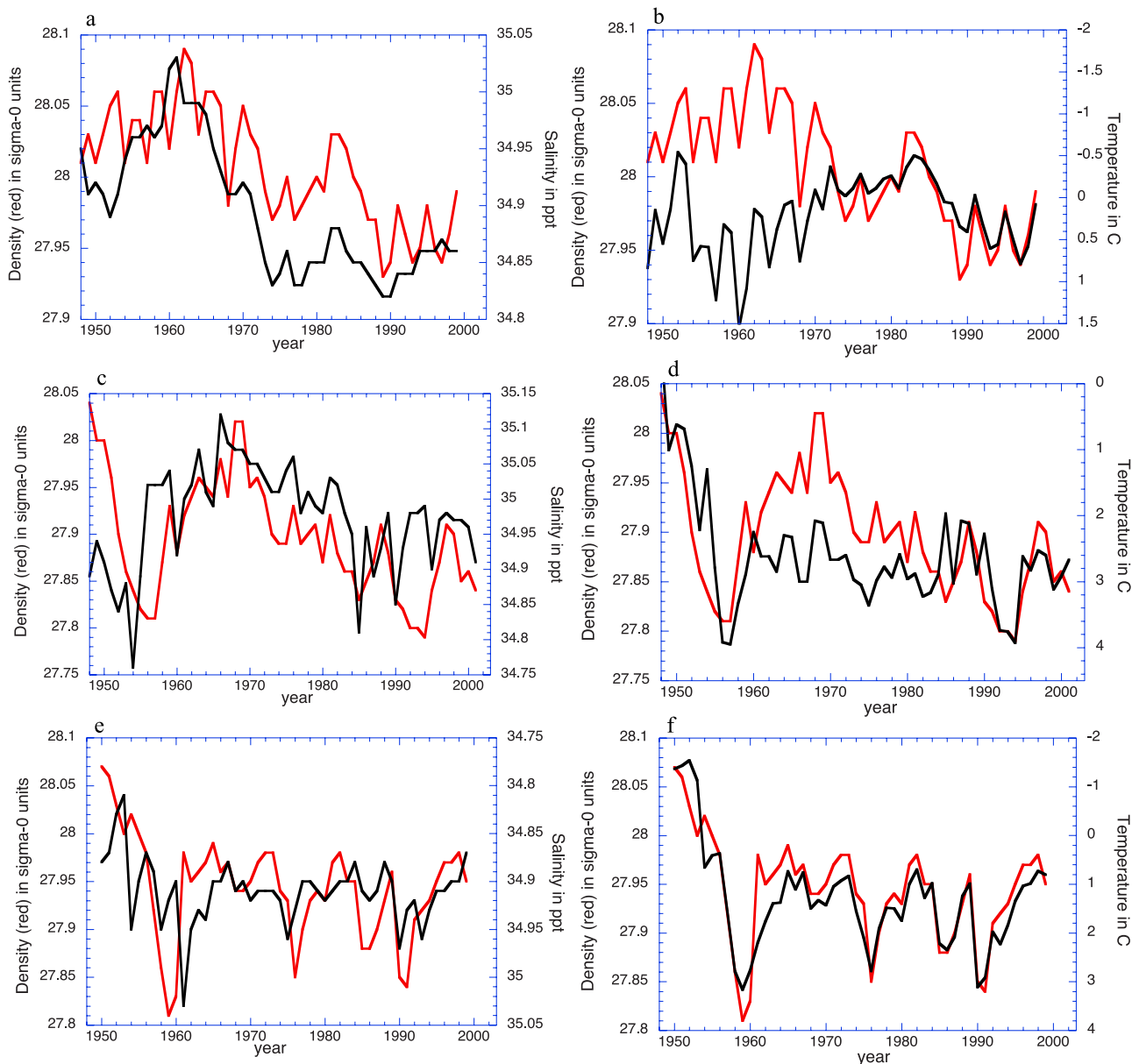
Figure 7. The maximum density (in red) fluctuations at 75°N (within the longitude band 10°W–15°E) and the associated salinity and/or temperature. From the AWI model: (a) S and RHO and (b) T and RHO. From the GSFC model: (c) S and RHO and (d) T and RHO. From the UL model: (e) S and RHO and (f) T and RHO. From the UW model: (g) S and RHO and (h) T and RHO. Observational relationships of density with salinity and with temperature are shown in (i) and (j), respectively. There are observational data gaps for the years 1951, 1956, 1960, 1963, 1966–1968, 1971, 1974, 1978, 1983, 1985, and 1992.
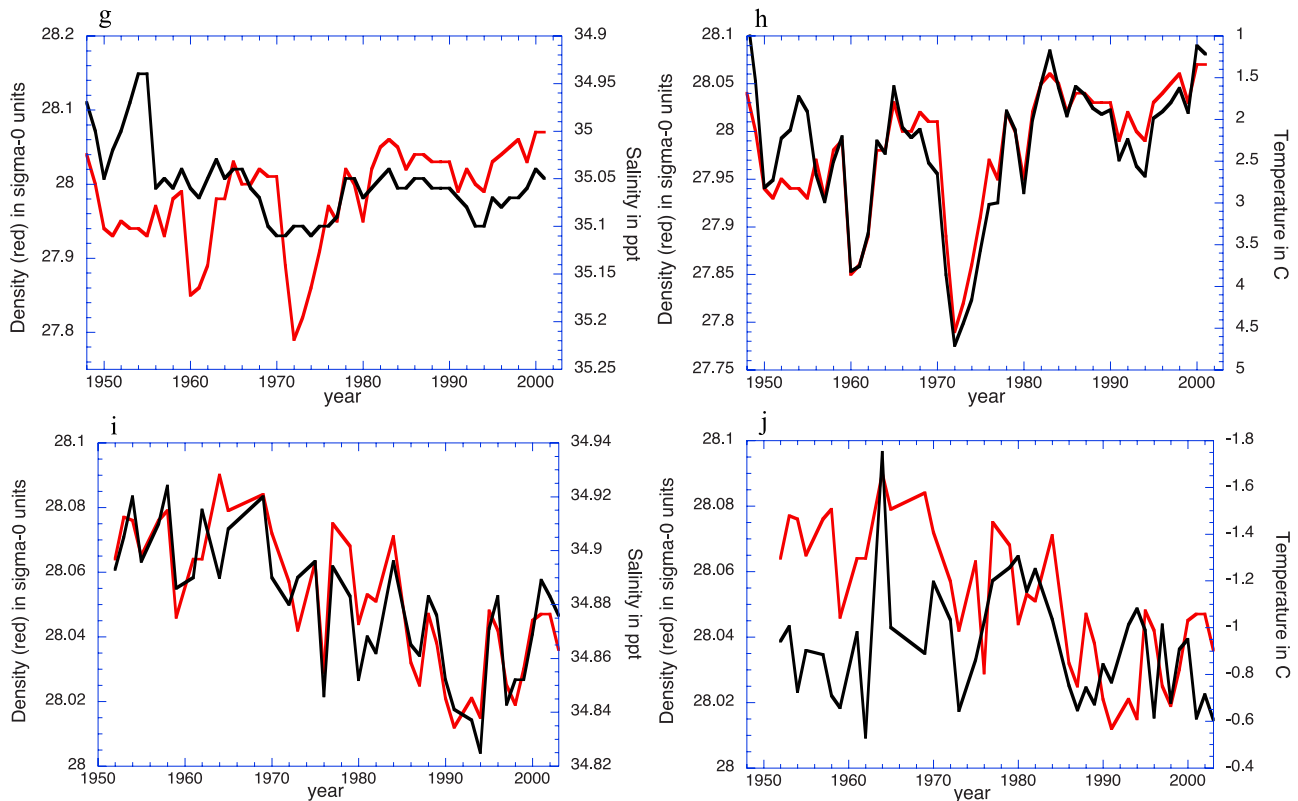
Figure 7. (continued)

importance of advection. The spatial patterns of this ratio are important in gauging the modification of Atlantic Water in the models. In the AWI model Atlantic Water undergoes the most severe cooling once it has started its southward path, where almost all of the lost heat must be brought in by advection. In the GSFC model the largest flux occurs before the Atlantic Water submerges under the Arctic ice cover near Spitzbergen. The UL model is similar to the AWI model with a path of high values with more evenly distributed heat loss along the Atlantic Water path.

[19] Figure 9e provides another perspective on the role of advection. Here GSFC model results are used for sea surface temperature (SST) and surface heat flux, which are plotted against Atlantic Water temperature (from Figure 8a). The SST and heat flux cover a much larger area (5–15°E, 70–80°N) and are averaged annually. The point measurement of temperature at 200 m at 15°E, 75°N reflects rather well a much larger regional temperature variability that is dominated by the Atlantic Water. The notable difference between SST and heat flux variability, especially at longer time scales, is
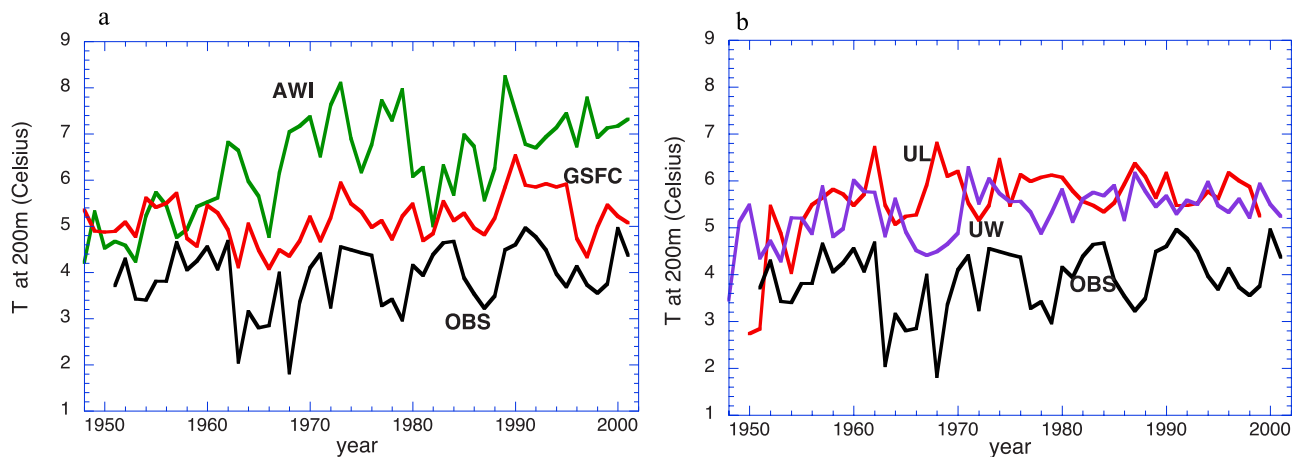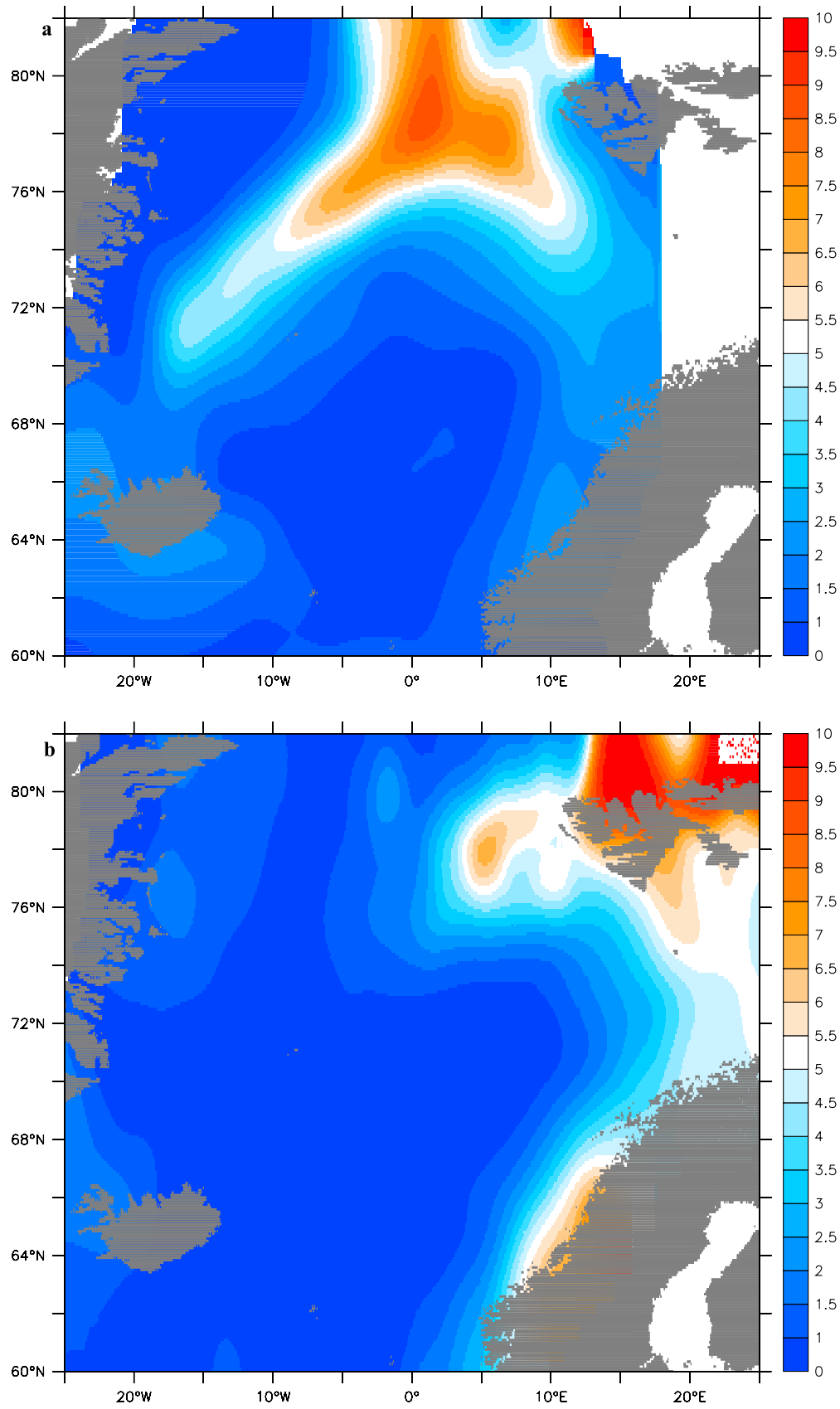

Figure 8. Temperature time series at 200 m from 73.5°N–76.5N, 15°E (i.e., the incoming Atlantic water): (a) the AWI and GSFC model data versus observed temperature (OBS, black; data gap in 1974 filled by interpolation). (b) UL, UW model data versus observations.

Figure 9. Ratio of winter heat loss over summer heat gain from the AWI (a), GSFC (b), UL (c), and UW (d) models for the years 1955–1999. Ratios much larger than one indicate heat advection to be a significant term in the heat balance. (e) Annual average SST and heat flux from 5–20°E, 70–80°N together with T at 200 m, (15°E, 75°N). Positive heat flux values denote heat loss.
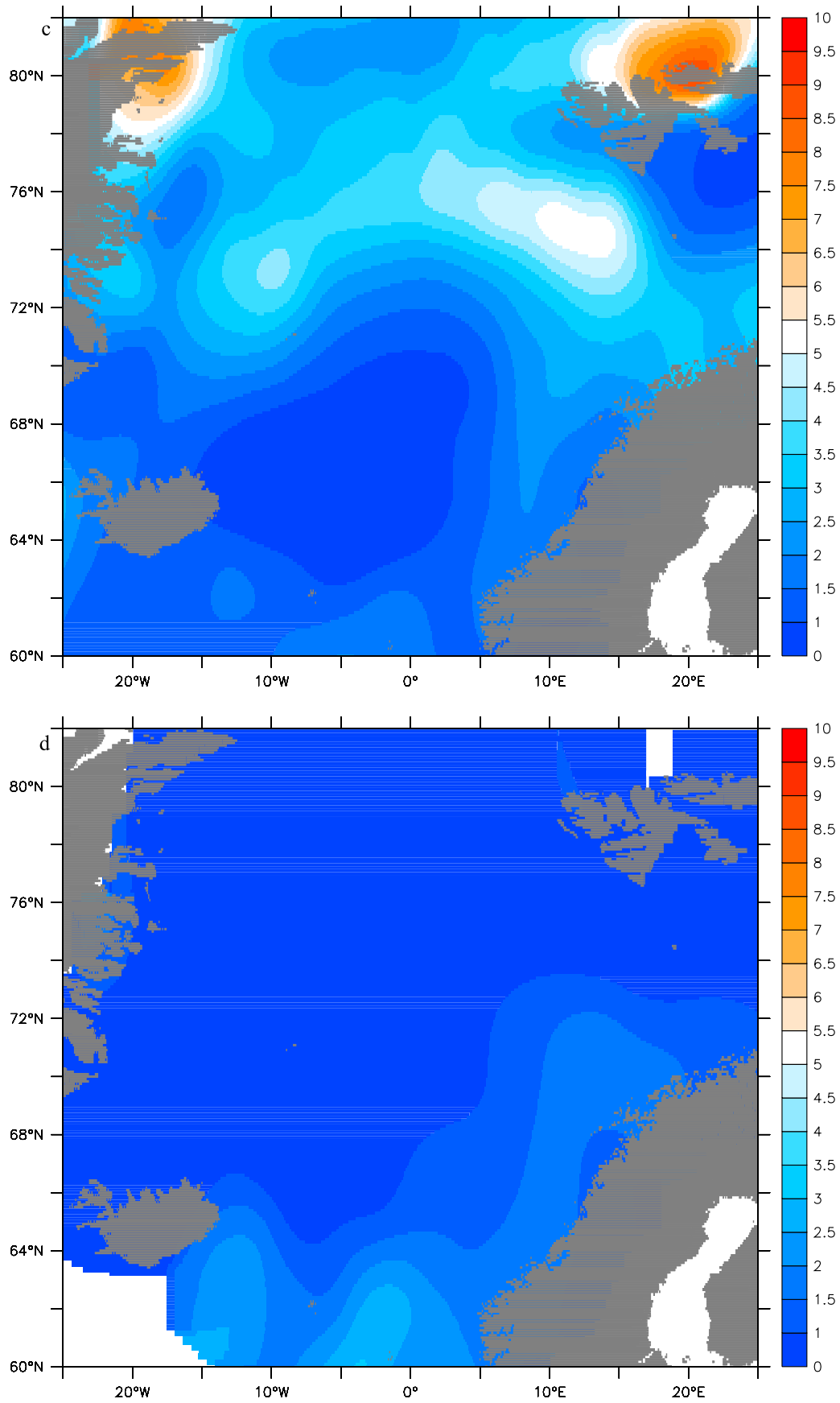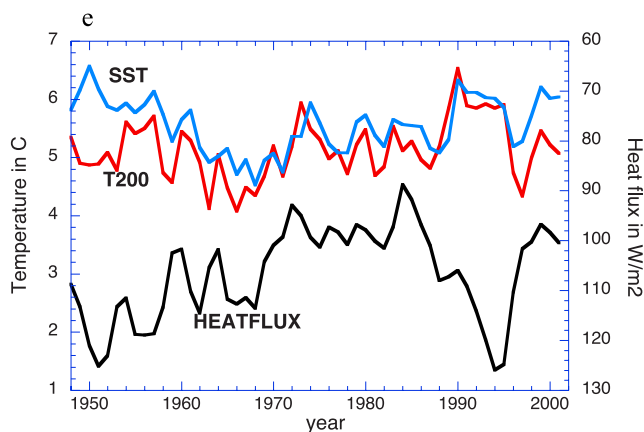
Figure 9. (continued)

Figure 9. (continued)

the relationship between heat flux and SST: A warm SST anomaly is associated with a heat loss anomaly (and not with a heat gain anomaly). This emphasizes the advection of heat to the region and deemphasizes the impact of local heat flux. The 1950s, 1960s, and 1990s behavior of SST and heat flux are the most apparent examples of heat-advection dominance.

[20] Detailed variations of Atlantic Water salinity (at 200/234 m, 15°E, 75°N) are shown in Figures 10a and 10b. While the overall salinity in the GSFC model is in the range of observed variability, the fluctuations are not well correlated with observations. The UW model is the only one to reach a significant correlation with observations (0.40), but the model leads by one year. At a model grid point scale (25 km to 100 km) advection of salt is more important to the salt balance than local fluxes, because the atmosphere does not damp salinity anomalies as it does temperature anomalies. Over the whole distance from the Nordic Sills to Spitzbergen (~1000 km), the impact from local precipitation and runoff and from the fresh Arctic origin infusion via the East Icelandic Current [*Blindheim et al.*, 2000] sets up a background salinity gradient. However, even a moderate salinity anomaly entering the Nordic Seas could be difficult to modify by local surface flux anomalies. As an example,

we consider a salinity anomaly (ΔS) of 0.1 ppt over the 200-m water column entering at the Nordic Sills. Assuming a mean northward current v of 10 cm/s, mean salinity along the 1000-km path of S = 35.2 ppt and minimal vertical exchange of salt at 200 m, we seek to find the amount of anomalous salt flux per unit area needed to remove the salinity anomaly by equating:

$$v \times \Delta S / 1000 \text{ km} = |R| S / 200 \text{ m},$$

where R is the freshwater/saltwater flux to the 200-m column. With the above values, |R| needs to be about 1.7 m/y. Considering present estimates of 2 mm/day (= 0.7 m/y) of net precipitation near the Norwegian Coast, the required freshwater/saltwater flux anomaly is unrealistically large for a P-E anomaly. This example demonstrates the overwhelming importance of salt advection in salt balance, but it also explains why anomalies like the Great Salinity Anomaly can survive for long distances. So, focusing on the passage of the 1960s Great Salinity Anomaly and the second salinity anomaly centered at 1988, none of the models timed them well. The UW model, with information on the inflowing salinity variability (from a global version of the same model), was slightly more successful than the others, but with a temporal offset. Based on the considerations above, simulation of Atlantic Water salinity in the Nordic Seas requires a robust simulation of local circulation such as that of the East Iceland Current, which brings fresh Arctic-origin and ice-melt waters to the Norwegian Sea [*Blindheim et al.*, 2000]. Beyond the local dynamics, a critical salinity evolution before the Atlantic Water reaches the Greenland Sea is the inflow salinity at the Nordic Sills, which is determined by circulation changes in the main North Atlantic [*Hátún et al.*, 2005].

5. Summary

[21] This study surveys simulated hydrographic properties for the Greenland-Iceland-Norwegian Seas from a range of models using either z- or sigma-levels in the vertical, a C or B grid in the horizontal, and a range of resolutions in the horizontal plane. All four ice-ocean models surveyed were
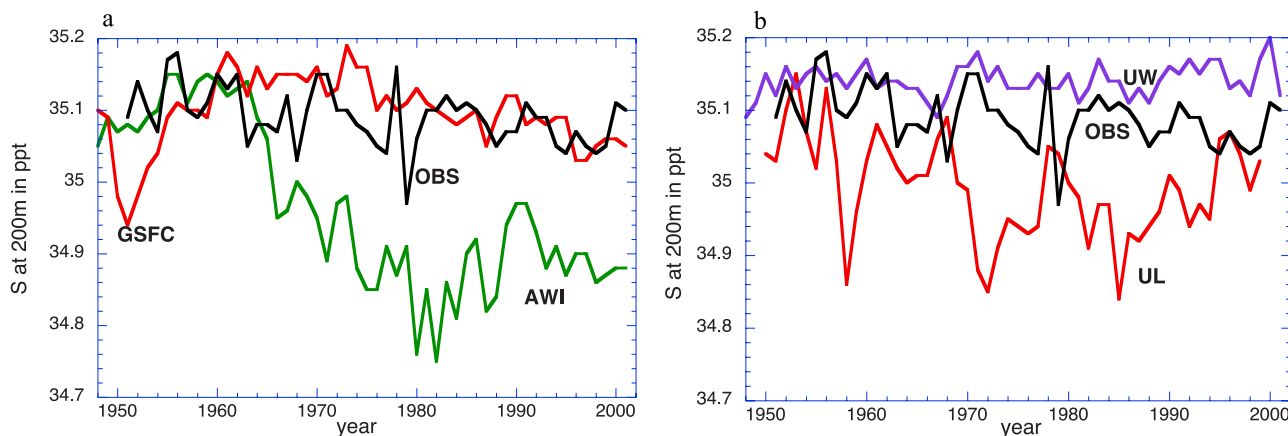

Figure 10. Salinity time series at 200 m from 73.5−76.5°N, 15°E: (a) the AWI and GSFC model data versus observed salinity (OBS, black; data gap in 1974 filled by interpolation). (b) UL and UW model data versus observations.

subjected to forcing as specified by the AOMIP project. It should be noted that these four are only a small sample of models used by the high-latitude oceanographic community. There likely exist models that perform better (or worse) under the same surface forcing, and likewise these four models are known to perform better with a different choice of restoring of surface salinity [e.g., *Gerdes et al.*, 2003; *Drange et al.*, 2005], surface forcing, and model domain (e.g., extended to the global domain or to the tropical Atlantic). While the focus is on model intercomparison, observed data are used to gauge model success. The primary objective is to analyze the space and time variability of simulated upper-ocean temperature, salinity, and density at 200 or 234 m, which are used as a proxy for winter mixed layer properties, and to identify time periods when the upper-ocean waters were the densest. Such periods are likely to coincide with periods of deep convection in the Greenland Sea.

[22] The temperature, salinity, and density fields were investigated with respect to their mutual dependence regionally and their time evolution. The mutual correlations between salinity, temperature, and density fluctuations depict in principle the intrinsic properties of the water masses and their circulation. Time evolution at 75°N, particularly the evolution of Atlantic Water characteristics, exposes deficiencies of the experimental setups. One source of deficiency identified is the large role of advection in salt and heat balance along the track of Atlantic Water. Advection-associated changes can originate both from outside and inside the Nordic Seas to control the evolution of water masses together with the local thermohaline forcing. *Hátún et al.* [2005] show that the salinity of the Atlantic inflow to the Nordic Seas is controlled by the strength of the subpolar gyre, which by contracting and expanding controls the mixture of Atlantic Water entering through the Faroe Current. *Kauker et al.* [2005] show that temperature and salinity anomalies generated at 50°N, in contrast to barotropic fluctuations originating there, can easily be transported into the Nordic Seas. However, they also find that anomalies generated locally in the Nordic Seas can be of the same order as anomalies propagating within the North Atlantic Current. *Blindheim et al.* [2000] show that lateral mixing with Arctic waters is particularly active in the Norwegian Sea where the extension of the East Iceland Current brings very fresh waters. Model results point to a conclusion that the T-S evolution in the interior of the Greenland-Iceland-Norwegian Seas depends on the boundary conditions at the Nordic Sills, as evidenced by success of the UW and GSFC models for Atlantic Water temperature evolution. However, salinity evolution remains problematic in all four models, even in the UW and GSFC models, which receive their boundary information from a much larger domain (see Table 1). The location of the southern boundary south of the Nordic Sills and including most of the subpolar gyre into the model domain, as in the AWI and the UL models, is not adequate to prevent a drift. The apparent requirement for boundary information (for both hydrography and momentum fluxes) from the main North Atlantic Ocean is based on the importance of meridional overturning changes in the high latitude (north of 45°N) salt balance [*Häkkinen*, 2002]. It is also evident that further improvement to Nordic Seas simulation can be

provided by higher resolution in order to capture the detailed topographically controlled circulation patterns (as evidenced by the AWI and UW models).

[23] These comparisons show that modeling the Nordic Seas-Arctic system must undergo significant improvements in order to simulate the system's evolution realistically. Based on a short, 50-year record of observations, we can establish intrinsic relationships of the water masses, although we have no information about how the system behaves on a much longer-term basis, over hundreds to thousands of years. One property in question is the salinity-dominated maximum density of the upper ocean in the central Greenland Sea, which was successfully simulated by two of the models, although one of them switches from a salinity-dominated regime to a temperature-dominated regime. In the two other models the density maximum was determined by the coldest temperature. These differences reflect interactions of locally and remotely forced thermohaline effects on water masses which are strongly steered by topography. Increasing model resolution will likely help to account for strong topographic control on circulation. This should also improve simulations of high-latitude stratification where advection of heat and salt is an important part of local heat and salt balance. Research is also needed in the area of surface fluxes, since at present the matching of model setup and forcing data sets from observations is a matter of either gamble or tuning, while surface restoring involves damping feedbacks. One probable way out of this dilemma may be introduction of flux correction (see *Köberle and Gerdes* [2007] for a discussion). It is also apparent that the Nordic Seas are not insulated from main North Atlantic influences, which suggests the need to expand beyond regional Nordic Seas–Arctic models.

References

Blindheim, J., and S. Osterhus (2005), *The Nordic Seas: Main Oceanographic Features*, pp. 11–38, AGU, Washington, D. C.

Blindheim, J., V. Borokov, B. Hansen, S. A. Malmberg, W. R. Turrell, and S. Osterhus (2000), Upper layer cooling and freshening in the Norwegian Sea in relation to atmospheric forcing, *Deep Sea Res., Part I*, *47*, 655–680.

Blumberg, A. F., and G. L. Mellor (1987), A description of a three-dimensional coastal ocean circulation model, in *Three Dimensional Coastal Ocean Models*, edited by N. S. Heaps, pp. 1–16, AGU, Washington, D. C.

Bonisch, G., J. Blindheim, J. L. Bullister, P. Schlosser, and D. W. R. Wallace (1997), Long-term trends of temperature, salinity, density and transient tracers in the Greenland Sea, *J. Geophys. Res.*, *102*(C8), 18,553–18,571.

Budeus, G., W. Schneider, and G. Krause (1998), Winter convective events and bottom water warming in the Greenland Sea, *J. Geophys. Res.*, *103*(C9), 18,513–18,527.

Dickson, R. R., J. Meincke, S.-A. Malmberg, and A. J. Lee (1988), The "Great Salinity Anomaly" in the northern North Atlantic, 1968–1982, *Prog. Oceanogr.*, *20*, 103–151.

Drange, H., R. Gerdes, Y. Gao, M. Karcher, F. Kauker, and C. Koberle (2005), *Ocean General Circulation Modeling of the Nordic Seas*, pp. 199–220, AGU, Washington, D. C.

Gerdes, R., M. Karcher, F. Kauker, and U. Schauer (2003), Causes and development of repeated Arctic Ocean warming events, *Geophys. Res. Lett.*, *30*(19), 1980, doi:10.1029/2003GL018080.

GSP Group (1990), The Greenland Sea Project—A venture toward improved understanding of the ocean's role in climate, *Eos Trans. AGU*, *71*, 750–751, 754–755.

Häkkinen, S. (2002), Surface salinity variability in the northern North Atlantic during recent decades, *J. Geophys. Res.*, *107*(C12), 8003, doi:10.1029/2001JC000812.

Häkkinen, S. (2007), Upper ocean T-S variations in the Greenland Sea and their association to climatic conditions, *J. Geophys. Res.*, doi:10.1029/2006JC003498, in press.

Häkkinen, S., and C. A. Geiger (2000), Simulated low frequency modes of circulation in the Arctic Ocean, *J. Geophys. Res.*, *105*, 6549–6564.

Häkkinen, S., and G. L. Mellor (1992), Modeling the seasonal variability of the coupled Arctic ice-ocean system, *J. Geophys. Res.*, *97*, 20,285–20,304.

Hátún, H., B. Hansen, A. B. Sandø, H. Drange, and H. Valdimarsson (2005), De-stabilization of the North Atlantic Thermohaline Circulation by a Gyre Mode, *Science*, *309*, 1841–1844.

Holloway, G., and T. Sou (2002), Has Arctic sea ice rapidly thinned?, *J. Clim.*, *15*, 1691–1701.

Holloway, G., et al. (2007), Water properties and circulation in Arctic Ocean models, *J. Geophys. Res.*, *112*, C04S03, doi:10.1029/2006JC003642.

Karcher, M., R. Gerdes, F. Kauker, and C. Köberle (2003), Arctic warming: Evolution and spreading of the 1990s warm event in the Nordic Seas and the Arctic Ocean, *J. Geophys. Res.*, *108*(C2), 3034, doi:10.1029/2001JC001265.

Karcher, M., F. Kauker, R. Gerdes, E. Hunke, and J. Zhang (2007), On the dynamics of Atlantic Water circulation in the Arctic Ocean, *J. Geophys. Res.*, *112*, C04S02, doi:10.1029/2006JC003630.

Karstensen, J., P. Schlosser, D. W. R. Wallace, J. L. Bullister, and J. Blindheim (2005), Water mass transformation in the Greenland Sea during the 1990s, *J. Geophys. Res.*, *110*, C07022, doi:10.1029/2004JC002510.

Kauker, F., R. Gerdes, M. Karcher, and C. Koeberle (2005), Impact of North Atlantic Current changes on the Nordic Seas and the Arctic Ocean, *J. Geophys. Res.*, *110*, C12002, doi:10.1029/2004JC002624.

Köberle, C., and R. Gerdes (2007), Simulated variability of the Arctic Ocean fresh water balance 1948–2001, *J. Phys. Oceanogr.*, in press.

Lammers, R. B., and A. I. Shiklomanov (2000), R-ArcticNet: A regional hydrographic data network for the pan-Arctic region, Water Syst. Anal. Group, Univ. of N. H., Durham.

Osterhus, S., and T. Gammelsrod (1991), The abyss of the Nordic Seas is warming, *J. Clim.*, *12*, 3297–3304.

Polyakov, I. V., et al. (2005), One more step toward a warmer Arctic, *Geophys. Res. Lett.*, *32*, L17605, doi:10.1029/2005GL023740.

Rasmusson, E. M., and K. Mo (1996), Large scale atmospheric moisture cycling as evaluated from NMC global analysis and forecast products, *J. Clim.*, *9*, 3276–3297.

Rhein, M. (1991), Ventilation rates of the Greenland and Norwegian Seas derived from distributions of the chloro fluoromethanes F11 and F12, *Deep Sea Res.*, *38*, 485–503.

Rhein, M. (1996), Convection in the Greenland Sea, 1982–1993, *J. Geophys. Res.*, *101*(C8), 18,183–18,192.

Rosati, A., and K. Miyakoda (1988), A general-circulation model for upper ocean simulation, *J. Phys. Oceanogr.*, *18*(11), 1601–1626.

Schlosser, P., G. Bonisch, M. Rhein, and R. Bayer (1991), Reduction of deep water formation in the Greenland Sea during the 1980s: Evidence from tracer data, *Science*, *251*, 1054–1056.

Steele, M., R. Morley, and W. Ermold (2001), PHC: A global ocean hydrography with a high quality Arctic Ocean, *J. Clim.*, *14*, 2079–2087.

Xie, P. P., and P. A. Arkin (1996), Analyses of global monthly precipitation using gauge observations, satellite estimates, and numerical model predictions, *J. Clim.*, *9*, 840–858.

Zhang, J., and D. A. Rothrock (2003), Modeling global sea ice with a thickness and enthalpy distribution model in generalized curvilinear coordinates, *Mon. Weather Rev.*, *131*(5), 681–697.

Zhang, J., and M. Steele (2007), Effect of vertical mixing on the Atlantic Water layer circulation in the Arctic Ocean, *J. Geophys. Res.*, *112*, C04S04, doi:10.1029/2006JC003732.

Zhang, J., D. A. Rothrock, and M. Steele (2000), Recent changes in Arctic sea ice: The interplay between ice dynamics and thermodynamics, *J. Clim.*, *13*, 3099–3114.

———————————

F. Dupont, Quebec-Ocean, Université Laval, Sainte-Foy, QC, Canada G1K 7P4.

S. Häkkinen, NASA Goddard Space Flight Center, Greenbelt, MD 20771, USA. (sirpa.hakkinen@nasa.gov)

M. Karcher and F. Kauker, Alfred Wegener Institute for Polar and Marine Research, D- 27515 Bremerhaven, Germany.

D. Worthen, Science Systems and Applications Inc., 10210 Greenbelt Road, Suite 600, Lanham, MD 20706, USA.

J. Zhang, Applied Physics Laboratory, University of Washington, 1013 NE 40th Street, Seattle, WA 98105, USA.